Chapter 10
Casimir Forces and Near-Field Radiative Heat Transfer in Graphene Structures

Casimir has shown that quantum fluctuations of the electromagnetic field produce an attractive force between macroscopic bodies. It has recently been shown that two non-contacting bodies moving relative to each other experience a friction due to the same quantum fluctuations of the electromagnetic field. However, until recently, there was no experimental evidence for or against this effect, because the predicted friction forces are very small, and precise measurements of quantum forces are incredibly difficult with the presently available technology. The existence of quantum friction is still debated even among theoreticians. However, the situation drastically changed with the discovery of a new material—graphene. We recently proposed that quantum friction can be detected in frictional drag experiments between graphene sheets, and in the transport properties of non-suspended graphene on an SiO_2 substrate in a high electric field.

Here, we investigate the dependence of the thermal Casimir force and the Casimir friction force between two graphene sheets on the drift velocity of the electrons in one graphene sheet. We show that the drift motion produces a measurable change of the thermal Casimir force due to the Doppler effect. The thermal Casimir force, as well as the Casimir friction, are strongly enhanced in the case of resonant photon tunneling when the energy of the emitted photon coincides with the energy of electron–hole pair excitations. In the case of resonant photon tunneling, even for temperatures above room temperature, the Casimir friction is dominated by quantum fluctuations.

We have used the theories of the Casimir friction and the near-field radiative energy transfer to study the heat generation and dissipation in graphene due to the interaction with phonon–polaritons in the (amorphous) SiO_2 substrate and acoustic phonons in graphene. For the low-field (low drift velocity) energy transfer between non-suspended graphene and the substrate, radiative energy transfer gives a significant contribution in addition to the phononic heat transfer. High-field (large drift velocity) heat transfer is determined by the phononic mechanism. For high electric field (large drift velocities) and low temperatures, quantum fluctuations give an important contribution to the energy flux and the friction force. For suspended graphene, the energy transfer coefficient at nanoscale gap is $\sim$3 orders of magnitude larger than the radiative heat transfer coefficient of the blackbody radiation limit. We

A.I. Volokitin and B.N.J. Persson, *Electromagnetic Fluctuations at the Nanoscale*,
NanoScience and Technology, DOI 10.1007/978-3-662-53474-8_10

have pointed out that graphene can be used to study near-field radiative heat transfer in the plate–plate configuration, and for shorter separations than is currently possible in the plate–sphere configuration.

10.1 Introduction

Friction is usually a very complicated process. It appears in its most elementary form when two flat surfaces, separated by a vacuum gap, are sliding relative to each other at zero Kelvin, where the friction is generated by the relative movement of quantum fluctuations. For several decades, physicists have been intrigued by the idea of quantum friction. It has recently been shown that two non-contacting bodies moving relative to each other experience a friction due to quantum fluctuations inside the bodies [11, 115, 121, 128]. However, until recently, there was no experimental evidence for or against this effect, because the predicted friction forces are very small, and precise measurements of quantum friction are incredibly difficult with presently available technology. Recently, we proposed [149, 165] that using graphene it should be possible to detect quantum friction.

Graphene, isolated monolayer of carbon, which was obtained very recently [270], consists of carbon atoms densely packed into a 2D honeycomb crystal lattice (Fig. 10.1). The unique electronic and mechanical properties of graphene are actively studied both theoretically and experimentally partly because of their importance for fundamental physics, and also because of its possible technological applications [270–273]. In particular, the valence band and conduction band in graphene touch each other, at one point named the Dirac point. Near this point, the energy spectrum for electrons and holes has a linear dispersion. Due to this linear (or 'conical') dispersion relation, electrons and holes near this point behave like relativistic particles described by the Dirac equation for massless fermions.

Graphene can also be useful for the detection of quantum friction. Consider graphene located on the surface of, for example, the polar dielectric SiO_2, or nearby on a second graphene sheet. In this case, the charge carriers in graphene experience

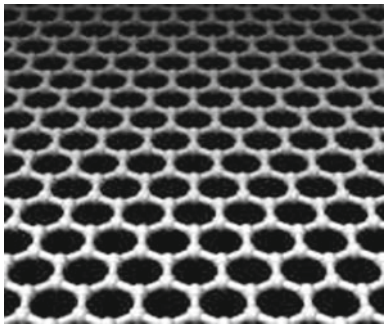

Fig. 10.1 Honeycomb lattice of graphene

additional friction due to interaction with the optical phonons in the dielectric, or the electrons in the other graphene sheet. Due to the high mobility, in a strong electric field the electrons in graphene can move with very high drift velocities ($\sim 10^6$ m/s). At such velocities, the main contribution to the friction will arise from quantum fluctuations. Thus, quantum friction can be detected by measuring the high electric field transport properties of graphene on a polar dielectric substrate, or by measuring the voltage induced by friction in a second nearby graphene sheet.

10.2 The Casimir Forces in Graphene Systems

At present, a great deal of attention is devoted to the study of the Casimir forces in graphene systems [274–282]. This is due to the unusual electronic properties of graphene, which result in Casimir forces with unusual properties. For normal materials, the contribution to the Casimir force due to thermal fluctuations dominates for $d > \lambda_T$; but, for two graphene sheets, the thermal contribution dominates of much shorter distances [282] $d > \xi_T = \hbar v_F / k_B T$, where $v_F \sim 10^6$ m/s is the Fermi velocity in graphene. At room temperature, the parameters λ_T and ξ_T are 7.6 μm and 25 nm, respectively. This property makes it possible to measure the thermal Casimir force using an atomic force microscope, or other force-measuring techniques. Tailoring the thermal Casimir force using Fermi level tuning by gate voltage was discussed in [280].

An alternative method of tailoring the thermal Casimir force consists of driving an electric current in a graphene sheet. It was shown by Pendry [115] that the reflection amplitudes from a moving metal surface are modified due to the Doppler effect. The same modification of reflection amplitudes can be obtained if, instead of the motion of a metal plate, a drift motion of charge carriers is induced in it by applied voltage [283]. The drift motion of the charge carries in graphene will result in a modification of dielectric properties (and the Casimir force) of graphene due to the Doppler effect [115] (see Fig. 1.7). If, in one of two parallel graphene sheets, an electric current is induced, then the electromagnetic waves, radiated by the graphene sheet without an electric current, will experience a frequency Doppler shift in the reference frame moving with the drift velocity v of electrons in the other graphene sheet: $\omega' = \omega - q_x v$, where q_x is the parallel to the surface component of the momentum transfer. The same is true for the waves emitted by the other graphene sheet. Due to the frequency dependence of the reflection amplitudes, the electromagnetic waves will reflect differently in comparison with the case when there is no drift motion of electrons, and this will give rise to the change of the Casimir force. The effect of the drift motion of charge carriers in one of the graphene sheet, on the thermal Casimir force between graphene sheets, was investigated in [165].

Let us consider two graphene sheets separated by a vacuum gap with thickness $d \ll \lambda_T$. Assume that the free charge carriers in one graphene sheet move with drift velocity $v \ll c$ along the x-axis (c is the light velocity) relative to the other graphene sheet. Because a drift motion of the free charge carriers produces a similar

modification of the reflection amplitudes as in the case of moving graphene sheet, the theory of the Casimir forces between moving bodies [128] can be used to calculate the Casimir forces between the sheets (both of which are at the rest) in the presence of the drift motion of the free charge carriers in one graphene sheet. The force, which acts on the surface of the sheet, can be calculated from the Maxwell stress tensor σ_{ij}, evaluated at the surface of the sheet at $z = 0$:

$$\sigma_{ij} = \frac{1}{4\pi}\int_0^\infty d\omega \int \frac{d^2q}{(2\pi)^2}\Big[\Big\langle E_i E_j^*\Big\rangle + \Big\langle E_i^* E_j\Big\rangle + \Big\langle B_i B_j^*\Big\rangle + \Big\langle B_i^* B_j\Big\rangle - \delta_{ij}\Big(\langle \mathbf{E}\cdot\mathbf{E}^*\rangle + \langle \mathbf{B}\cdot\mathbf{B}^*\rangle\Big)\Big]_{z=0} \tag{10.1}$$

where $\langle ...\rangle$ denotes statistical average over the fluctuating electromagnetic field. According to [128], the Casimir force $F_z = \sigma_{zz}$ between the moving media is determined by

$$F_z = F_{zT} + F_{z0}, \tag{10.2}$$

where the temperature-dependent term F_{zT}, and the zero-temperature contribution F_{z0} are given by

$$F_{zT} = \frac{\hbar}{\pi^3}\int_0^\infty dq_y \int_0^\infty dq_x q e^{-2qd} \Bigg\{\int_0^\infty d\omega\Bigg(\frac{\mathrm{Im}R_1(\omega)\mathrm{Re}R_2(\omega^+)n_1(\omega) + \mathrm{Re}R_1(\omega)\mathrm{Im}R_2(\omega^+)n_2(\omega^+)}{\mid 1 - e^{-2qd}R_1(\omega)R_2(\omega^+)\mid^2} + (1\leftrightarrow 2)\Bigg) + \int_0^{q_x v} d\omega\Bigg(\frac{\mathrm{Re}R_1(\omega^-)\mathrm{Im}R_2(\omega)n_2(\omega)}{\mid 1 - e^{-2qd}R_1(\omega^-)R_2(\omega)\mid^2} + (1\leftrightarrow 2)\Bigg)\Bigg\}, \tag{10.3}$$

$$F_{z0} = \frac{\hbar}{2\pi^3}\int_0^\infty dq_y \int_0^\infty dq_x \Bigg\{\mathrm{Re}\int_0^\infty d\omega s e^{-2sd}\Bigg(\frac{R_1(i\omega)R_2(i\omega + q_x v)}{1 - e^{-2sd}R_1(i\omega)R_2(i\omega + q_x v)} + (1\leftrightarrow 2)\Bigg) + \int_0^{q_x v} d\omega q e^{-2qd}\Bigg(\frac{\mathrm{Im}R_1(\omega)\mathrm{Re}R_2(\omega^-)}{\mid 1 - e^{-2qd}R_1(i\omega)R_2(\omega^-)\mid^2} + (1\leftrightarrow 2)\Bigg)\Bigg\}, \tag{10.4}$$

where $n_i(\omega) = [\exp(\hbar\omega/k_B T_i) - 1]^{-1}$ $(i = 1, 2)$, $q = \sqrt{q_x^2 + q_y^2}$, $s = \sqrt{(\omega/c)^2 + q^2}$, T_i is the temperature of i-th graphene sheet, R_i is the reflection amplitude for surface i for p-polarized electromagnetic waves, and $\omega^\pm = \omega \pm q_x v$. The symbol $(1 \leftrightarrow 2)$ denotes the terms that are obtained from the preceding terms by permutation of 1 and 2. In the first term in (10.4), the integration along the real axis was transformed into an integration along the imaginary axis.

The reflection amplitude for a 2D system is determined by [144]

$$R_i = \frac{\epsilon_i - 1}{\epsilon_i}, \quad \epsilon_i = \frac{2\pi p \sigma_i}{\omega \varepsilon} + 1, \tag{10.5}$$

where $p = \sqrt{(\omega/c)^2 - q^2}$, σ_i is the longitudinal conductivity of the sheet, which can written in the form $\sigma_i = -i\omega e^2 \Pi_i(\omega, q)/q^2$ where Π_i is the 2D polarizability. The dielectric function of the sheet is determined by $\varepsilon_i(\omega, q) = 1 + v_q \Pi_i(\omega, q)$ where $v_q = 2\pi e^2/(q\varepsilon)$ is the 2D Coulomb interaction. In terms of ε_i the reflection amplitude can be written as

$$R_i = \frac{p(\varepsilon_i - 1)}{p(\varepsilon_i - 1) + iq} \tag{10.6}$$

In the integration on the real axis $p \approx iq$ for $d < \lambda_T$. Thus, in this case

$$R_i \approx \frac{\varepsilon_i - 1}{\varepsilon_i}, \tag{10.7}$$

On the imaginary axis, $p = is$. In the finite lifetime generalization according to the Mermin approximation [354], the dielectric function is determined by

$$\varepsilon(\omega, q) \approx 1 + \frac{(\omega + i\gamma)\big(\varepsilon_0(\omega + i\gamma, q) - 1\big)}{\omega + i\gamma\big(\varepsilon_0(\omega + i\gamma, q) - 1\big)/\big(\varepsilon_0(0, q) - 1\big)}, \tag{10.8}$$

where $\varepsilon_0(\omega, q)$ is the RPA dielectric function and γ is the damping parameter. In the study below, we used the dielectric function of graphene, which was calculated recently within the random-phase approximation (RPA). The small (and constant) value of the graphene Wigner-Seitz radius r_s indicates that it is a weakly interacting system for all carries densities, making the RPA an excellent approximation for graphene (RPA is asymptotically exact in the $r_s \ll 1$ limit). The dielectric function is an analytical function in the upper half-space of the complex ω-plane:

$$\varepsilon_0(\omega, q) = 1 + \frac{4k_F e^2}{\hbar v_F q} - \frac{e^2 q}{2\hbar\sqrt{\omega^2 - v_F^2 q^2}}\left\{G\left(\frac{\omega + 2v_F k_F}{v_F q}\right) - G\left(\frac{\omega - 2v_F k_F}{v_F q}\right) - i\pi\right\}, \tag{10.9}$$

where

$$G(x) = x\sqrt{x^2 - 1} - \ln\left(x + \sqrt{x^2 - 1}\right), \tag{10.10}$$

where the Fermi wave vector $k_F = (\pi n)^{1/2}$, n is the concentration of charge carriers, the Fermi energy $\epsilon_F = \hbar v_F k_F$, $v_F \approx 10^6$ m/s is the Fermi velocity. The damping parameter γ is due to electron scattering against impurities and acoustic phonons in graphene sheet, and can be expressed through the low-field mobility μ: $\gamma = ev_F/(\hbar k_F \mu)$. Scattering of the graphene carries by the acoustic phonons of graphene places an intrinsic limits on the low-field room temperature ($T_0 = 300$

K) mobility, given by $\mu_0 = 20$ m^2/Vs at the graphene carriers density 10^{16} m^{-2} (see [357]), which gives $\gamma = 8 \times 10^{11}$ s^{-1}. At other temperatures the mobility can be obtained using the relation $\mu = \mu_0 T_0/T$.

In addition to the intrinsic friction due to scattering against impurities and phonons, during drift motion of the electrons in the graphene sheet, the extrinsic friction occurs due to the interaction with the electrons in the nearby graphene sheet. According to the theory of the Casimir friction [128], the friction force $F_x = \sigma_{xz} = F_{xT} + F_{x0}$, where at $d \ll \lambda_T$ and $v \ll c$ the contributions from thermal (F_{xT}) and quantum (F_{x0}) fluctuations are given by [11, 115, 121, 149]

$$F_{xT} = \frac{\hbar}{\pi^3}\int_0^\infty dq_y \int_0^\infty dq_x q_x e^{-2qd} \left\{ \int_0^\infty d\omega \left(\frac{\mathrm{Im}R_1(\omega)\mathrm{Im}R_2(\omega^+)}{|\,1 - e^{-2qd}R_1(\omega)R_2(\omega^+)\,|^2} \times \left[n_1(\omega) - n_2(\omega^+) \right] + (1 \leftrightarrow 2) \right) - \int_0^{q_x v} d\omega \left(\frac{\mathrm{Im}R_1(\omega)\mathrm{Im}R_2(\omega^-)}{|\,1 - e^{-2qd}R_1(\omega)R_2(\omega^-)\,|^2} n_1(\omega) + (1 \leftrightarrow 2) \right) \right\}, \tag{10.11}$$

$$F_{x0} = -\frac{\hbar}{2\pi^3}\int_0^\infty dq_y \int_0^\infty dq_x q_x e^{-2qd} \int_0^{q_x v} d\omega \left(\frac{\mathrm{Im}R_1(\omega)\mathrm{Im}R_2(\omega^-)}{|\,1 - e^{-2qd}R_1(\omega)R_2(\omega^-)\,|^2} + (1 \leftrightarrow 2) \right). \tag{10.12}$$

Equations (10.11) and (10.12) were initially obtained for 3D systems in [115] at $T = 0$ and in [121] for finite temperatures. However, in [144] it was shown that the same formulas are valid for 2D systems. For $v < dk_B T/\hbar$ (at $d = 1$ nm and $T = 300$ K for $v < 4 \times 10^4$ m/s) the main contribution to the friction (10.11) depends linearly on the sliding velocity v so that the friction force $F_{xT} = \Gamma v$, where at $T_1 = T_2 = T$ the friction coefficient Γ is given by

$$\Gamma = \frac{\hbar^2}{8\pi^2 k_B T}\int_0^\infty \frac{d\omega}{\sinh^2\left(\frac{\hbar\omega}{2k_B T}\right)} \int_0^\infty dq\, q^3 e^{-2qd} \frac{\mathrm{Im}R_1(\omega)\mathrm{Im}R_2(\omega)}{|\,1 - e^{-2qd}R_1(\omega)R_2(\omega)\,|^2}. \tag{10.13}$$

Due to the presence of an exponential factor in the expression (10.3) for the thermal contribution to the Casimir force, the integration over frequency is effectively limited to $\omega < \omega_T = k_B T/\hbar$. Thus, for $q_x v \sim v/d > \omega_T$ (at room temperature and for $d = 1$ nm, this condition corresponds to the velocities $v > 10^5$ m/s), the integrand will be modified in the whole range of integration, which will give rise to the significant change of the thermal Casimir force. This change will be especially large in the case of resonant photon tunneling when the integrand has sharp resonances. The integrand in the expression for the zero-temperature contribution to the Casimir force does not contain any sharp cut-off in the frequency integration. Thus, the range of integration will be wider and the change of the zero-temperature contribution will be significant only for much higher velocities than for the thermal contribution.

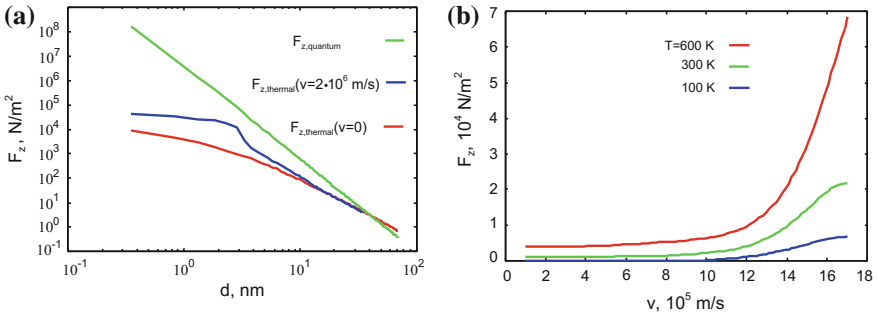

Fig. 10.2 The Casimir forces between two graphene sheets with carrier concentration $n = 10^{16}\text{m}^{-2}$. **a** The dependence of the Casimir force on the separation d between the sheets. The thermal and quantum contributions to the total Casimir force are shown separately. The thermal contribution is shown for $T = 600$ K and for the drift velocities $v = 0$ and $v = 2 \times 10^6$ m/s; **b** The dependence of the thermal Casimir force on the drift velocity of electrons v in one of the graphene sheet at $d = 1$ nm

Figure 10.2a shows the dependence of the Casimir force between two graphene sheets on the separation, d, between the sheets. The thermal and quantum contributions are shown separately. The thermal contribution was calculated for $T = 600$ K and for the electron drift velocities $v = 0$ and $v = 2 \times 10^6$ m/s. The thermal contribution becomes larger than the quantum contribution for $d > 50$ nm. For $d < 5$ nm, the thermal contribution calculated for $v = 2 \cdot 10^6$ m/s is significantly larger then the thermal contribution calculated at $v = 0$. For example, at $d \approx 3$ nm the drift motion of the electrons gives rise to an increase of the thermal Casimir force by one order of magnitude, and in this case the thermal contribution is only one order of magnitude smaller than the quantum contribution, and can be measured experimentally. Figure 10.2b shows the dependence of the thermal Casimir force F_{zT} on the drift velocity of the electrons in the graphene sheet at $d = 1$ nm. Note the significant change of the thermal Casimir force for $v/d > \omega_T$ (at room temperature and for $d = 1$ nm, this condition corresponds to the velocities $v > 10^5$ m/s).

Let us assume that in the rest reference frame, in which there is no drift motion of electrons, an electron hole pair excitation has the energy $\omega_{eh}(q)$ and momentum $\mathbf{q}$, then in the laboratory reference frame, in which the electron system is moving with drift velocity v, due to the Doppler effect, the energy of this excitation will be equal to $\omega_{eh}(q) - q_x v$. For $v > \omega_{eh}(q)/q_x$ the excitation energy will be negative. Thus, for velocities larger than critical velocity ($v_{cr} = \omega_{eh}(q)/q_x$), as a result of such excitation, the photon can be created with energy $\omega_{ph}(q) = q_x v - \omega_{eh}(q) > 0$, i.e. radiation arises. This radiation is reminiscent of the Cherenkov radiation, which arises when an electron moves in a medium with a velocity exceeding the light velocity in the medium. The difference between the two phenomena is that Cherenkov radiation is connected to the radiation of electromagnetic waves, but the radiation which arises from drift motion of the electron in the graphene sheet results from the excitations of electron–hole pairs in graphene. Resonance arises

when the photon emitted by the moving electron system in one graphene sheet with energy $\omega_{ph}(q) = q_x v - \omega_{eh}(q) > 0$ will create excitation with energy $\omega_{eh}(q)$ in the other graphene sheet. In the case of graphene, the energy of the electron hole pair excitation $\omega_{eh}(q) \approx v_F q$, where v_F is the Fermi velocity. Thus, resonance arises when $q_x v \approx 2v_F q$, which requires that $v > 2v_F \approx 2 \times 10^6$ m/s, in accordance with the numerical calculations.

10.3 Using Graphene to Detect Quantum Friction

Quantum friction determines the ultimate limit to which the friction can be reduced. In order to detect quantum friction, it is necessary to reduce the contribution to friction from other mechanisms up to unprecedented levels. However, even in non-contact friction experiments [166, 359], when two bodies are not in direct contact, there are several contributions to the friction [11]. Moreover, quantum friction dominates over thermal friction at velocities $v > dk_B T/\hbar$ (at $d = 1$ nm and room temperature: $v > 10^5$m/s). However, at present, even for a hard cantilever, the velocity of the tip cannot exceed 1 m/s [359].

We recently proposed [149] that it should be possible to detect quantum friction in graphene adsorbed on an amorphous SiO_2 substrate (Fig. 10.3). The electrons, moving in graphene under the action of an electric field, will experience an intrinsic friction due to interaction with the acoustic and optical phonons in graphene, and an extrinsic friction due to interaction with the optical phonons in the SiO_2-substrate. In high electric fields, the electrons move with high velocities, and in this case the main contribution to the friction arises from the interaction with the optical phonons in graphene and in SiO_2. However, the frequency of the optical phonons in graphene is approximately four times larger than in SiO_2. Therefore, the main contribution to the friction will result from the interaction with the optical phonons in SiO_2. Thus, this frictional interaction determines the electrical conductivity of graphene at high electric field.

The dissipated energy due to the friction results in heating of the graphene, and is transferred to the SiO_2 substrate via the near-field radiative heat transfer process and direct phononic coupling. Using the theories of Casimir friction and the near-field radiative heat transfer, we have formulated a theory that describes these phenomena and allows us to predict experimentally measurable effects. In comparison with the existing microscopic theories of transport in graphene [360, 361], our theory is macroscopic. The electromagnetic interaction between graphene and a substrate is described by the dielectric functions of the materials, which can be accurately determined from theory and experiment.

Let us consider graphene and a substrate with flat parallel surfaces at separation $d \ll \lambda_T = c\hbar/k_B T$. Assume that the free charge carriers in graphene move with the velocity $v \ll c$ (c is the light velocity) relative to the substrate. According to [11, 121, 128], the frictional stress F_x acting on the charge carriers in graphene, and the radiative heat flux S_z across the surface of substrate, both mediated by a fluctuating

electromagnetic field, are determined by

$$F_x = \frac{\hbar}{\pi^3}\int_0^\infty dq_y \int_0^\infty dq_x q_x e^{-2qd}\left\{\int_0^\infty d\omega\left(\frac{\mathrm{Im}R_d(\omega)\mathrm{Im}R_g(\omega^+)}{|\,1-e^{-2qd}R_d(\omega)R_g(\omega^+)\,|^2}\right.\right.$$
$$\times\left[n_d(\omega)-n_g(\omega^+)\right]+\left.\frac{\mathrm{Im}R_d(\omega^+)\mathrm{Im}R_g(\omega)}{|\,1-e^{-2qd}R_d(\omega^+)R_g(\omega)\,|^2}\left[n_g(\omega)-n_d(\omega^+)\right]\right)$$
$$\left.+\int_0^{q_x v} d\omega\frac{\mathrm{Im}R_d(\omega)\mathrm{Im}R_g(\omega^-)}{|\,1-e^{-2qd}R_d(\omega)R_g(\omega^-)\,|^2}\left[n_g(\omega^-)-n_d(\omega)\right]\right\}, \tag{10.14}$$

$$S_z = \frac{\hbar}{\pi^3}\int_0^\infty dq_y \int_0^\infty dq_x e^{-2qd}\left\{\int_0^\infty d\omega\left(\frac{\omega\mathrm{Im}R_d(\omega)\mathrm{Im}R_g(\omega^+)}{|\,1-e^{-2qd}R_d(\omega)R_g(\omega^+)\,|^2}\right.\right.$$
$$\times\left[n_d(\omega)-n_g(\omega^+)\right]+\left.\frac{\omega^+\mathrm{Im}R_d(\omega^+)\mathrm{Im}R_g(\omega)}{|\,1-e^{-2qd}R_d(\omega^+)R_g(\omega)\,|^2}\left[n_g(\omega)-n_d(\omega^+)\right]\right)$$
$$\left.+\int_0^{q_x v} d\omega\frac{\omega\mathrm{Im}R_d(\omega)\mathrm{Im}R_g(\omega^-)}{|\,1-e^{-2qd}R_d(\omega)R_g(\omega^-)\,|^2}\left[n_g(\omega^-)-n_d(\omega)\right]\right\}, \tag{10.15}$$

where $n_i(\omega)=[\exp(\hbar\omega/k_BT_i-1]^{-1}\,(i=g,d)$, $T_{g(d)}$ is the temperature of graphene (substrate), R_i is the reflection amplitude for surface i for p-polarized electromagnetic waves, and $\omega^\pm=\omega\pm q_x v$. The reflection amplitude for graphene is determined by (10.7) and for the substrate

$$R_d=\frac{\epsilon_d-1}{\epsilon_d+1}, \tag{10.16}$$

where ϵ_d is the dielectric function for substrate. The dielectric function of amorphous SiO_2 can be described using an oscillator model [358]

$$\epsilon(\omega)=\epsilon_\infty+\sum_{j=1}^{2}\frac{\sigma_j}{\omega_{0,j}^2-\omega^2-i\omega\gamma_j}, \tag{10.17}$$

where parameters $\omega_{0,j}$, γ_j and σ_j were obtained by fitting the measured ϵ for SiO_2 to the above equation, and are given by $\epsilon_\infty=2.0014$, $\sigma_1=4.4767\times10^{27}\mathrm{s}^{-2}$, $\omega_{0,1}=8.6732\times10^{13}\mathrm{s}^{-1}$, $\gamma_1=3.3026\times10^{12}\mathrm{s}^{-1}$, $\sigma_2=2.3584\times10^{28}\mathrm{s}^{-2}$, $\omega_{0,2}=2.0219\times10^{14}\mathrm{s}^{-1}$, and $\gamma_2=8.3983\times10^{12}\mathrm{s}^{-1}$.

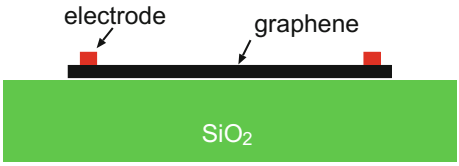

Fig. 10.3 Scheme of the graphene field effect transistor

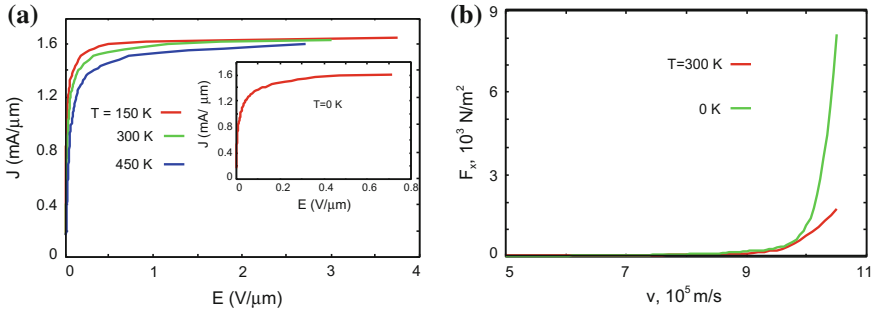

Fig. 10.4 The role of the interaction between phonon polaritons in SiO_2 and free carriers in graphene for graphene field-effect transistor transport. The separation between graphene and the SiO_2 is $d = 3.5$ Å, and the charge density $n = 10^{12}$ cm^{-12} **a** Current density-electric field dependence for different temperatures. *Inset* shows the same dependence at $T = 0$ K; **b** Dependence of the quantum and thermal contributions to the friction force (per unit area) between SiO_2 and the free carriers in graphene per unit area on the drift velocity of electrons in graphene. The finite temperature curve shows only the thermal contribution

The steady-state temperature can be obtained from the condition that the power generated by friction must be equal to the energy transfer across the substrate surface

$$F_x(T_d, T_g)v = S_z(T_d, T_g) + \alpha_{ph}(T_g - T_d), \tag{10.18}$$

where the second term in (10.18) takes into account the heat transfer through direct phononic coupling; α_{ph} is the thermal contact conductance due to phononic coupling.

Figure 10.4a shows the dependence of the current density on the electric field at the carrier concentration $n = 10^{12}$ cm^{-2}, and for different temperatures. We have found that, in agreement with the experiment [164], the current density saturates at $E \sim 0.5$–2.0 V/μm. According to the experiment, the saturation current density $J_{sat} = nev_{sat} \approx 1.6$ mA/μm, and using the charge density concentration $n = 10^{12}$ cm^{-2}: $v_{sat} \approx 10^6$ m/s. The saturation current density depends weakly on the temperature. In Fig. 10.4b, the contributions to the friction force from quantum and thermal fluctuations are shown separately. In the saturation region, the contribution to the friction force from quantum fluctuations dominates.

According to the theory of the Casimir friction [11] (see also above discussion), the quantum friction, which exists even at zero temperature, is determined by the creation of excitations (electron hole pairs or optical phonons) in each of the interacting media. The frequency of the photon associated with the excitations in moving body is determined by $\omega_{ph} = vq_x - \omega_1$, where ω_1 is the excitation frequency in the rest reference frame. This photon will create excitation in the other body with the frequency $\omega_2 = \omega_{ph} = vq_x - \omega_1$. The relevant excitations in graphene are the electron–hole pairs with energy $\omega_{eh}(q) \approx v_F q$, while for SiO_2 the frequency of surface phonon polaritons $\omega_0 \approx 60$ meV (9×10^{13} s^{-1}). Resonant photon tunneling occurs at $v > v_F + \omega_0/q_x$. The maximal value of wave vector is $\sim 1/d$. Thus, at $d = 0.35$ nm, resonance occurs for $v > v_{sat} = v_F + \omega_0 d \sim 10^6$ m/s, in accordance

with the numerical calculations. Thus, measurements of the current density–electric field relation of graphene adsorbed on SiO_2 provide the possibility of detecting quantum friction.

10.4 Casimir Frictional Drag Force Between Graphene Sheets

An alternative method of studying Casimir friction consists of driving an electric current in one metallic layer and studying the effect of the frictional drag on the electrons in a second (parallel) metallic layer (Fig. 9.1). Such experiments were proposed by Pogrebinskii [255] and Price [256], and were performed for 2D quantum wells [112–114]. In these experiments, a current is driven through layer **1**. Due to the proximity of the layers, the interlayer interactions will induce a current in layer **2** due to a frictional stress acting on the electrons in the layer **2** from layer **1**. If the layer **2** is an open circuit, an electric field E_1 will develop in the layer whose influence cancels the frictional stress σ between the layers. In the experiment [112], the drift velocity $v \sim 10^2$ m/s. According to the theory of the Casimir friction [121, 144], at such velocities, the thermal fluctuation gives the dominant contribution to the friction, and the theoretical predictions are in agreement with experiment.

Frictional drag between graphene sheets was measured recently in [162, 163]. This study has fueled the recent theoretical investigations of frictional drag between graphene sheets [362–368] mediated by a fluctuating Coulomb field. In all of these investigations, the current density (or drift velocity v of the charge carries) is linearly related to the driving electric field. Thus, only the thermal contribution to the frictional drag was included. In the linear approximation, the electric field induced by the frictional drag depends linearly on the current density $J = nev$ (or drift velocity v of the charge carries), $E = \rho_D J = F_{xT}/ne = \Gamma J/(ne)^2$, where Γ is the friction coefficient and $\rho_D = \Gamma/(ne)^2$ is the drag resistivity. For $\omega < v_F q$ and $q < 2k_F$ the dielectric function of graphene has the following form [356]

$$\varepsilon_0(\omega, q) \approx 1 + \frac{4e^2 k_F}{\hbar v_F q}\left(1 + i\frac{\omega}{v_F q}\right), \tag{10.19}$$

and the reflection amplitude

$$R_0(\omega, q) = \frac{\varepsilon_0(\omega, q) - 1}{\varepsilon_0(\omega, q)} \approx 1 + i\frac{\hbar\omega}{4e^2 k_F}, \tag{10.20}$$

and (10.20) and (10.13) give the known result [362]

$$\rho_D = \frac{\Gamma}{(ne)^2} = \frac{h}{e^2}\frac{\pi\zeta(3)}{32}\left(\frac{k_B T}{\epsilon_F}\right)^2 \frac{1}{(k_F d)^2}\frac{1}{(k_{TF} d)^2}, \tag{10.21}$$

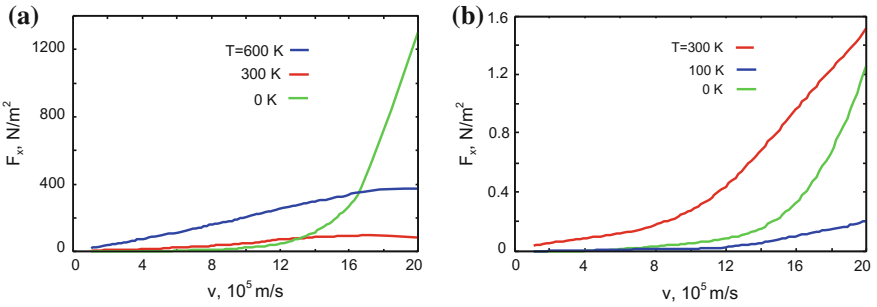

Fig. 10.5 Frictional drag between two graphene sheets at the carrier concentration $n = 10^{12}$ cm^{-2}. The finite temperature curves show only the thermal contributions to the friction. **a** Dependence of friction force between graphene sheets on the drift velocity of charge carriers in one graphene sheet at the layer separation $d = 1$ nm. **b** The same as in (**a**) but at $d = 10$ nm

where $k_{TF} = 4e^2 k_F/\hbar v_F$ is the Thomas-Fermi screening wave vector. The frictional drag force is much higher for high drift velocities ($\sim 10^6$ m/s), where it depends non-linearly on the drift velocity, and is dominated by the quantum friction [149]. For $v < v_F$ (10.20) and (10.12) give the following result for quantum friction

$$F_{x0} = \frac{\hbar v}{d^4}\frac{15\zeta(5)}{128\pi^2}\left(\frac{v}{v_F}\right)^2 \frac{1}{(k_{TF}d)^2}. \tag{10.22}$$

In the linear approximation $E = 5 \times 10^{-4} v$ (SI-units) for $T = 300$ K and $d = 10$ nm. For a graphene sheet of length 1 μm, and with $v = 100$ m/s, this electric field will induce the voltage $V = 10$ nV. From (10.21) and (10.22), the ratio between the quantum and thermal friction $F_{x0}/F_{xT} = F_{x0}/(ne)^2\rho_D v \approx (15/8\pi^2)(v/v_T)^2$, where $v_T = \omega_T d$. Thus, for $v > v_T$ the friction is dominated by quantum friction (at $d = 1$ nm and room temperature: $v_T \approx 4 \times 10^4$m/s).

Figure 10.5a, b show that much larger electric fields can be induced at $d = 1$ nm (a) and $d = 10$ nm (b) at large velocities. In these figures, the contributions to friction from thermal and quantum fluctuations are shown separately. For $v < 10^5$ m/s, the frictional drag effect for the graphene sheets strongly depends on temperature, i.e. it is determined mainly by the thermal fluctuations. However, for $v > 10^6$m/s it will be dominated by quantum fluctuations. Strong enhancement of friction occurs in the case of resonant photon tunneling. As discussed above, resonant photon tunneling occurs for $v > 2v_F \approx 2 \times 10^6$ m/s. For such velocities and $d = 1$ nm, quantum friction dominates over the thermal contribution even at room temperature (see Fig. 10.5a). For $d = 10$ nm, quantum friction dominates at low temperatures (see Fig. 10.5b).

The use of graphene in frictional drag experiments has considerable advantages in comparison with quantum wells. Such experiments can be performed in a vacuum where the contribution from the phonon exchange can be excluded. In a vacuum, one can easily measure the dependence of the frictional drag force on the separation between graphene sheets. Due to the high mobility of the charge carriers in graphene, the charge carriers can move with much higher drift velocity than in quantum wells.

10.5 Near-Field Radiative Heat Transfer Between Closely Spaced Graphene and Amorphous SiO_2

In this Section, we investigate heat generation and dissipation due to friction produced by the interaction between moving (drift velocity v) charge carriers in graphene and the optical phonons in a nearby amorphous SiO_2, and the acoustic phonons in graphene. Friction produces thermal heating of the graphene, which results in near-field radiative energy transfer and phononic heat transfer between the graphene and SiO_2. A self-consistent theory that describes these phenomena was formulated by us in [149] (see also Sect. 10.3) and it allows us to predict experimentally measurable effects. In comparison with the existing microscopic theories of energy transfer and transport in graphene [360, 361], our theory is macroscopic.

According to (10.14) and (10.15) in the case when free carriers are moving relative to the substrate both thermal and quantum fluctuations give contributions to the frictional stress and the radiative energy transfer. This situation is different from that considered in [370, 371] where it was assumed that the free carries in graphene had vanishing drift velocity. The contribution of the quantum fluctuations to the frictional stress was investigated by us in [149] (see also Sect. 10.3). According to (10.15) the contribution to the near-field energy transfer from quantum fluctuations is determined by

$$S_z^{quant} = S_z(T_d = T_g = 0) = -\frac{\hbar}{\pi^3}\int_0^\infty dq_y \int_0^\infty dq_x \int_0^{q_x v} d\omega \omega e^{-2qd} \frac{\mathrm{Im} R_d(\omega)\mathrm{Im} R_g(\omega^-)}{|\,1 - e^{-2qd} R_d(\omega) R_g(\omega^-)\,|^2} \tag{10.23}$$

As discussed in Sect. 10.3, for graphene on SiO_2 the excess heat generated by the current is transferred to the substrate through the near-field radiative heat transfer, and via the direct phononic coupling (for which the heat transfer coefficient $\alpha \approx 10^8 \mathrm{Wm}^{-2}\mathrm{K}^{-1}$). At small temperature difference ($\Delta T = T_g - T_d \ll T_d$), from (10.18) we get

$$\Delta T = \frac{F_{x0} v - S_{z0}}{\alpha_{ph} + S'_{z0} - F'_{x0} v} \tag{10.24}$$

where $F_{x0} = F_x(T_d, T_g = T_d)$, $S_{z0} = S_z(T_d, T_g = T_d)$,

$$F'_{x0} = \frac{dF_x(T_d, T_g)}{dT_g}\Big|_{T_g = T_d}, \quad S'_{z0} = \frac{dS_z(T_d, T_g)}{dT_g}\Big|_{T_g = T_d}$$

We note that, in contrast to the heat transfer between bodies at rest, for moving bodies the energy flux $S_z(T_d, T_g)$ is not equal to zero even for the case when there is no temperature difference between the bodies. The energy transfer coefficient is given by

$$\alpha = \frac{S_z(T_d, T_g) + \alpha_{ph}\Delta T}{\Delta T} \approx \frac{(\alpha_{ph} + S'_{z0})F_{x0}v - S_{z0}F'_{x0}v}{F_{x0}v - S_{z0}} \tag{10.25}$$

For small velocities $F_{x0} \sim v$ and $S_{z0} \sim v^2$. Thus, from (10.25) it follows that in the limit $v \to 0$ the energy transfer coefficient between moving bodies is not reduced to the heat transfer coefficient between bodies at rest, which is determined by $\alpha_{th} = \alpha_{ph} + S'_{z0}$. This effect is due to the term S_{z0} in the total energy flux which exists only between moving bodies. The energy transfer coefficient can be strongly enhanced in comparison with the heat transfer coefficient when $F_{t0}v \approx S_{z0}$. Figure 10.6a shows the ratio of the energy transfer coefficient to the phononic heat transfer coefficient for $d = 0.35\,\text{nm}$ and $n = 10^{16}\ \text{m}^{-2}$. For low and intermediate fields, this ratio is larger than unity, which means that, in this region, the near-fields radiative energy transfer gives an additional significant contribution to the heat transfer. For nonsuspended graphene on SiO_2, the energy and heat transfer are very effective and the temperature difference does not rise high, even for such high electric fields that saturation in $I - E$ characteristic starts [164] (see Fig. 10.6b). The

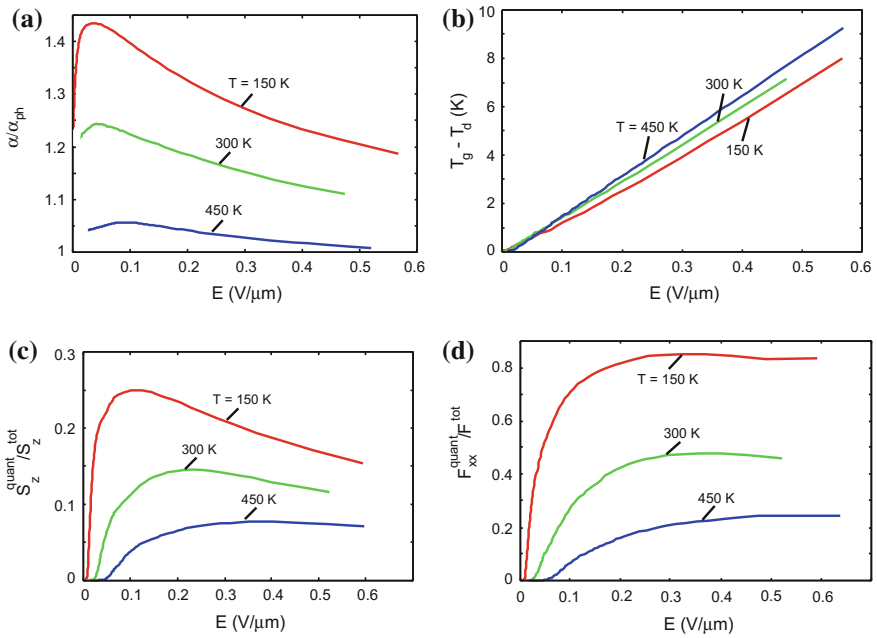

Fig. 10.6 Radiative energy transfer between graphene and SiO_2 for $n = 10^{16}\text{m}^{-2}$, $d = 0.35\,\text{nm}$ and $\alpha_{ph} = 1.0 \times 10^8 \text{Wm}^{-2}\text{K}^{-1}$. **a** The dependence of the ratio between the total energy transfer coefficient and the phononic heat transfer coefficient, on the electric field. **b** Dependence of the temperature difference between graphene and substrate on the electric field. **c** Dependence of the ratio between the heat flux only due to quantum fluctuations S_z^{quant} and the total energy flux, on the electric field. **d** Dependence of the ratio between the friction force due to quantum fluctuations F_x^{quant} and the total friction force, on the electric field

radiative heat transfer between bodies at rest is determined only by thermal fluctuations, in contrast to the radiative energy transfer between moving bodies, which is determined by both thermal and quantum fluctuations. Figure 10.6c shows that quantum fluctuations can give significant contribution to the total energy transfer for low temperatures and large electric field (high drift velocity). Similarly, in the (electric current) saturation region, quantum fluctuations give significant contribution to the total friction force which is determined, as discussed above, by the sum of the extrinsic and intrinsic friction forces (see Fig. 10.6d). The extrinsic friction force has contributions from both thermal and quantum fluctuations. The friction force due to quantum fluctuations is denoted as quantum friction, which was discussed in Sect. 10.3 (see also [149]).

Figure 10.7a shows the dependence of the energy transfer coefficient on the separation d for low electric field ($v \to 0$). At $d \sim 5$ nm and $T = 300$ K the energy transfer coefficient, due to the near-field radiative energy transfer, is $\sim 10^4\,\mathrm{Wm^{-2}K^{-1}}$, which is ∼three orders of magnitude larger than the radiative heat transfer coefficient due to

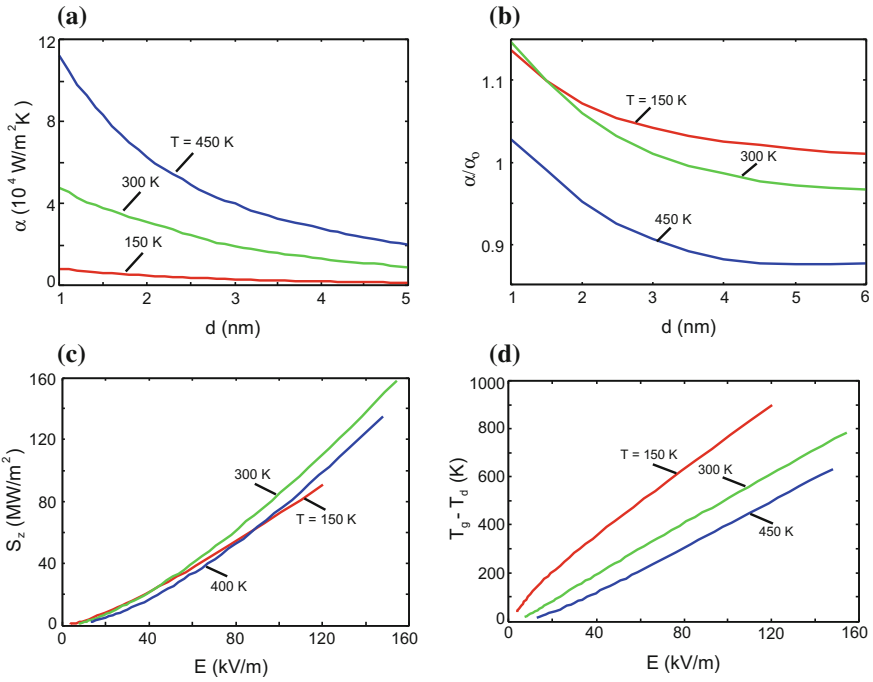

Fig. 10.7 Radiative energy transfer between graphene and SiO_2 for $n = 10^{12}\mathrm{cm^{-2}}$ and $\alpha_{ph} = 0$. **a** Dependence of the energy transfer coefficient on the separation d for low electric field ($v \to 0$); **b** Dependence of the ratio between the energy transfer coefficient and the heat transfer coefficient on the separation d for low electric field ($v \to 0$); **c** Dependence of the radiative energy flux on electric field for $d = 1.0$ nm; **d** Dependence of the temperature difference between graphene and substrate on electric field for $d = 1.0$ nm

the black-body radiation. In comparison, the near-field radiative heat transfer coefficient in the SiO_2–SiO_2 system for the plate–plate configuration, when extracted from experimental data [109] for the plate–sphere configuration, is $\sim 2230\,\mathrm{Wm^{-2}K^{-1}}$ at a ~ 30 nm gap. For this system, the radiative heat transfer coefficient depends on the separation as $1/d^2$. Thus $\alpha \sim 10^5\,\mathrm{Wm^{-2}K^{-1}}$ at $d \sim 5$ nm, which is one order of magnitude larger than for the graphene-SiO_2 system in the same configuration. However, the sphere has a characteristic roughness of ~ 40 nm, and the experiments [109, 110] were restricted to separation wider than 30 nm (at smaller separation the surface roughness affects the measured heat transfer). Thus, the extreme near-field-separation, with d less than approximately 10 nm, may not be accessible using a plate–sphere geometry. A suspended graphene sheet has a roughness ~ 1 nm [372], and measurements of the thermal contact conductance can be performed from separation larger than ~ 1 nm. At such separation one, would expect the emergence of non-local and non-linear effects. This range is of great interest for the design of nanoscale devices, as modern nanostructures are considerably smaller than 10 nm and are separated in some cases by only a few Angstroms.

Figure 10.7b shows that, at small separations, there is significant difference between the radiative energy transfer coefficient and the radiative heat transfer coefficient determined (in the absence of direct phononic coupling) by $\alpha_0 = S'_{z0}$. This difference vanishes for large separations because S_{z0} and F_{x0} rapidly decrease when the separation increases. At large separation, the friction force is dominated by the intrinsic friction and in this case $\alpha \approx \alpha_0$. Figure 10.7c shows the dependence of the radiative energy flux on electric field for $d = 1$ nm. For this separation, the energy transfer is considerably less effective than for $d = 0.35$ nm, which leads to a rapid increase of the temperature difference (see Fig. 10.7d). High temperatures are achieved at low electric field (small drift velocities), where contribution to the radiative energy transfer from quantum fluctuations is very small, and the energy transfer is mainly determined by thermal fluctuations.